

# Electron Bulk Heating at Saturn's Magnetopause

I Cheng<sup>1</sup>, N. Achilleos<sup>1</sup>, A. Masters<sup>2</sup>, G. Lewis<sup>1</sup>, M. Kane<sup>3</sup>, P. Guio<sup>1,4</sup>

<sup>1</sup>Department of Physics and Astronomy, University College London, London, UK

<sup>2</sup>Blackett Laboratory, Imperial College London, London, UK

<sup>3</sup>Harford Research Institute, Bel Air, MD, USA

<sup>4</sup>Department of Physics and Technology, Arctic University of Norway, Tromsø, Norway

## Key Points:

- Electron bulk heating at Saturn's magnetopause is used to test hypotheses about magnetic reconnection.
- Observations suggestive of locally open magnetopause tend to exhibit electron heating closer to the theoretical prediction for reconnection.
- $\Delta\beta$ -magnetic shear parameter space discriminates well between events with evidence of energisation and those without.

---

Corresponding author: I Cheng, [i.cheng.19@ucl.ac.uk](mailto:i.cheng.19@ucl.ac.uk)

## 14 **Abstract**

15 Magnetic reconnection at the magnetopause (MP) energises ambient plasma via the  
 16 release of magnetic energy and produces an “open” magnetosphere allowing solar wind  
 17 particles to directly enter the system. At Saturn, the nature of MP reconnection remains  
 18 unclear. The current study examines electron bulk heating at MP crossings, in order to  
 19 probe the relationship between observed and predicted reconnection heating proposed by  
 20 Phan et al. (2013) under open and closed MP, and how this may pertain to the position  
 21 of the crossings in the  $\Delta\beta$ -magnetic shear parameter space. The electron heating for 70  
 22 MP crossings made by the Cassini spacecraft from April 2005 to July 2007 was found  
 23 using 1d and 3d moment methods. Minimum variance analysis was used on the magnetic  
 24 field data to help indicate whether the MP is open or closed. We found better agreement  
 25 between observed and predicted heating for events suggestive of locally ‘open’ MP. For events  
 26 suggestive of locally ‘closed’ MP, we observed a cluster of points consistent with no electron  
 27 heating, but also numerous cases with significant heating. Examining the events in the  $\Delta\beta$ -  
 28 magnetic shear parameter space, we find 83% of events without evidence of energisation were  
 29 situated in the ‘reconnection suppressed’ regime, whilst between 43% to 68% of events with  
 30 energisation lie in the ‘reconnection possible’ regime depending on the threshold used. The  
 31 discrepancies could be explained by a combination of spatial and temporal variability which  
 32 makes it possible to observe heated electrons with different conditions from the putative  
 33 reconnection site.

## 34 **Plain Language Summary**

35 Saturn’s territory in space is marked by a boundary called the magnetopause. Particles  
 36 from the Sun can enter this region via a process called magnetic reconnection. However,  
 37 the conditions under which this process can occur on the boundary remains unclear. We  
 38 used the heating of electrons detected by the Cassini spacecraft during crossings of this  
 39 boundary to study the effects of different conditions on the viability of reconnection at  
 40 Saturn’s magnetopause. We found that most of the crossings which showed evidence of  
 41 significant electron heating close to theoretical predictions were also at locations where the  
 42 magnetopause was open (i.e. locations where solar particles can enter Saturn’s territory)  
 43 and /or where the local conditions were suitable for reconnection to take place.

## 44 **1 Introduction**

45 The magnetopause (MP) is the natural boundary of a planetary magnetosphere. It  
 46 is formed by the interaction between the solar wind and planetary magnetosphere. At  
 47 Saturn, it separates the magnetospheric magnetic field and plasma (mainly from the moon  
 48 Enceladus) from the solar wind interplanetary magnetic field (IMF) and plasma that has  
 49 to flow around the magnetospheric obstacle (Baines et al., 2018). Cassini observations of  
 50 magnetic field and plasma have also revealed that the disk-like magnetosphere imposes an  
 51 ‘inflation’ of the magnetopause at near-equatorial latitudes (Pilkington et al., 2014).

52 Magnetic reconnection is an important process at this boundary as it can energise  
 53 plasma via the release of magnetic energy when the fields undergo a topological change  
 54 to a lower energy state (Øieroset et al., 2001). The signature of this process is heated  
 55 high speed plasma jets (Yamada et al., 2010). Direct evidence of magnetic reconnection  
 56 signatures has been observed at Saturn’s magnetopause. For example, McAndrews et al.  
 57 (2008) reported two magnetopause crossings with heating in the electrons and ions along  
 58 field lines just outside the magnetopause that is highly suggestive of energisation comparable  
 59 to that associated with the reconnection process at Earth. Similarly, indirect evidence for  
 60 magnetopause reconnection based on ion dispersion signatures in the cusp region has been  
 61 reported by Jasinski et al. (2014).

62 In the absence of magnetic reconnection, the magnetosphere would be closed and thus  
 63 have no magnetic connection with the solar wind. The planetary magnetic field lines form  
 64 closed loops connecting one pole to the other (Figure 1). In this closed configuration, the  
 65 normal field component (i.e. the direction perpendicular to the local MP surface, also  
 66 the minimum variance direction for the magnetic field) is zero. However, under the right  
 67 conditions, the IMF embedded in the solar wind can reconnect with the planetary field. This  
 68 leads to an open magnetosphere with magnetic connection across the MP current layer where  
 69 solar wind plasma can directly enter the magnetosphere. Locally, the normal component  
 70 of the magnetic field relative to the MP surface becomes non-zero. This is illustrated in  
 71 Figure 1. The solar wind can couple with the magnetosphere via ‘large scale’ reconnection  
 72 and/or ‘viscous’ interaction like Kelvin-Helmholtz instabilities; the latter of which has been  
 73 suggested as the dominant mode at Saturn (Masters, 2018).

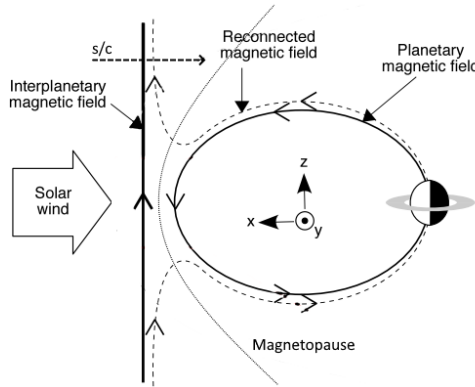


Figure 1: Schematic illustrating day side magnetic reconnection at Saturn’s magnetopause (dotted line) under northward IMF. The reconnected (open) magnetic field line is shown as dashed line. Adapted from Masters et al. (2012).

74 The question that arises is: Under what conditions is reconnection viable at Saturn’s  
 75 magnetopause? Swisdak et al. (2003) hypothesised that viable reconnection under a large  
 76 difference in plasma  $\beta$  (ratio of plasma to magnetic pressure) across the MP also requires  
 77 a high magnetic shear. Masters et al. (2012) analysed 70 magnetopause crossing events

at Saturn detected by the Cassini spacecraft and showed that the plasma  $\beta$  is higher in Saturn's magnetosheath (typically equal to 10) than in Earth's. This is believed to restrict reconnection to regions on the magnetopause with almost anti-parallel magnetic fields either side. Reconnection is suppressed when the following condition is satisfied:

$$|\Delta\beta| > \frac{2L}{d_i} \tan\left(\frac{\theta}{2}\right) \quad (1)$$

where  $L$  is the current layer thickness,  $d_i$  is the ion inertial length, and  $\theta$  is the magnetic shear angle across the current layer. This is the general diamagnetic suppression condition, introduced by Swisdak et al. (2010) and tested by Phan et al. (2010) using evidence from solar wind observations. Essentially, the theory suggests that a higher  $|\Delta\beta|$  across the current layer is less favourable for reconnection as the associated diamagnetic drift of charged particles can disrupt the reconnection jets.

In this paper, we use bulk electron heating (i.e. the scalar temperature change) at MP crossings ('events') as a possible reconnection signature to test the following hypotheses. 1) Events where the boundary is locally closed would have essentially no observed electron temperature change ( $\Delta T_e$ ) across the magnetopause, whereas most events with locally open boundary should have observed change close to the theoretical prediction. 2) Events with evidence of plasma heating should generally be in the 'reconnection possible' regime, whereas those without such evidence should lie in the 'reconnection suppressed' regime in the  $|\Delta\beta|$ -magnetic shear parameter space. This investigation examines the crossings from Masters et al. (2012) in more detail, in order to probe the relationship between observed and predicted  $\Delta T_e$ , and how this may pertain to the position of the crossings in the  $|\Delta\beta|$ -magnetic shear parameter space.

## 2 Cassini Data Set

The data set consists of 70 magnetopause (MP) crossings made by the Cassini spacecraft from April 2005 to July 2007, previously reported by Masters et al. (2012). These 70 events have full plasma  $\beta$  measurements including thermal  $\text{H}^+$  and  $\text{H}_2^+/\text{He}^{++}$  pressures on both sides of the MP and can be found in the original database in Masters et al. (2012).

For this study, magnetic field and particle data were used to further characterise the MP crossings. These measurements were obtained by the following two instruments on-board Cassini: The dual-technique magnetometer (MAG) (Dougherty et al., 2004), and the electron spectrometer (ELS) part of the CAPS (Cassini Plasma Spectrometer) instrument (Young et al., 2004). MAG provides the magnetic field measurements and 1-minute averaged data were used along with Kronocentric solar magnetospheric (KSM) coordinates, where  $X$  points from centre of Saturn to the Sun,  $Y$  points in the direction  $\Omega \times X$  (where  $\Omega$  is Saturn's rotational/magnetic dipole axis), and  $Z$  completes the right-handed coordinate system. Moments derived from 8-second averaged distributions in the ELS data provide electron density and temperature. The ELS instrument has eight anodes which sweeps through 63 bins covering an energy range of 0.58 eV to 26 keV in 2s. The ELS is able to

115 detect electron density as low as  $\sim 10^3 m^{-3}$  (Young et al., 2005). The field of view of each  
 116 anode is  $20^\circ \times 5^\circ$  (thus  $160^\circ \times 5^\circ$  for all eight anodes). An actuator sweeps the anodes back  
 117 and forth covering  $\sim 2\pi sr$  of solid angle. The coverage may be increased if the spacecraft  
 118 is rolling. For this study, we used anode 5 for all electron measurements as it has relatively  
 119 large pitch angle coverage (relative to the local magnetic field) throughout an actuation  
 120 cycle, compared to other anodes.

121 The MAG data were obtained from The Planetary Plasma Interactions (PPI) Node of  
 122 the Planetary Data System (PDS). The ELS and moments data were obtained from the  
 123 MSSL (Mullard Space Science Laboratory) server.

### 124 3 Methods

125 In this section, we describe our methodology used in the statistical survey to evaluate  
 126 the amount of bulk heating of magnetosheath electrons entering into the magnetopause  
 127 current layer (MPCL). We compare the observed heating ( $\Delta T_e$ ) to the theoretical bulk  
 128 heating due to reconnection based on inflow conditions (Phan et al., 2013), in an attempt to  
 129 determine whether the observed heating was potentially caused by magnetic reconnection  
 130 at Saturn’s magnetopause. Crucially, note that the theoretical value of  $\Delta T_e$  derived from  
 131 the data assumes that the observations are a faithful representation of the conditions at the  
 132 reconnection site. This is not necessarily the case; we discuss this point further, later in the  
 133 paper.

134 The crossing times and intervals of the 70 MP crossings previously reported by Masters  
 135 et al. (2012) were modified on a case by case basis for the purpose of this study. The inter-  
 136 vals were identified based on magnetic field rotation from the magnetosheath configuration  
 137 (usually weaker field) to the magnetosphere configuration (usually stronger field) in con-  
 138 junction with the electron moments showing signatures of transition from magnetosheath  
 139 (high density, low temperature) to magnetosphere (low density, high temperature). The  
 140 full plasma  $\beta$  measurements on both sides of the MPCL were from the original database in  
 141 Masters et al. (2012), while all other parameters were determined in this study.

142 For each event, the heating of magnetosheath electrons was calculated by subtracting  
 143 the average temperature in the pristine magnetosheath from that of the magnetosheath edge  
 144 of the magnetopause (‘exhaust’) i.e.  $\Delta T_{obs} = T_{exh} - T_{sh}$ . To achieve this, we required two  
 145 pieces of information: 1) A way to identify the ‘inner edge’ of the exhaust region. 2) A  
 146 reliable way of calculating the temperature of the magnetosheath electrons in each region.

147 To address the first requirement, Phan et al. (2013) used the ‘high-energy tail’ of an  
 148 electron energy spectrum as a means of detecting the first appearance of the magnetospheric  
 149 electron population and thus where the magnetosheath boundary layer (MSBL) ‘stops’. This  
 150 is the ‘inner edge’ of the exhaust, beyond which the magnetospheric population dominates.  
 151 If the temperature in the MSBL is significantly greater than that of the pristine magne-  
 152 tosheath, then it is said to be a heated magnetosheath population. To determine if this  
 153 heating is related to reconnection, we need to know whether the spacecraft is in an exhaust

154 signalled by enhanced velocity measurements (‘jets’) compared to the ambient plasma. How-  
 155 ever, bulk electron and ion velocity data are not available for most events as CAPS does not  
 156 normally view the entire  $4\pi$  steradians of solid angle due to three-axis stabilisation (stare  
 157 mode). Valid measurements of the plasma bulk velocity can only be obtained when the bulk  
 158 flow is in the field-of-view of CAPS (Arridge et al., 2009; Thomsen et al., 2010). The INCA  
 159 sensor measurements on the MIMI instrument of Cassini were successfully used to derive  $O^+$   
 160 plasma flow speeds in Saturn’s magnetosphere (Kane et al., 2020). However, this method  
 161 requires relatively stable conditions for usually 30 minutes; as such, boundaries where con-  
 162 ditions tend to be more variable were avoided. Based on this limitation, we proceeded with  
 163 determining the inner edge of the exhaust as above (i.e. Phan et al’s ‘tail’ method) but in  
 164 the absence of velocity data. Note that this inner edge could only be considered the location  
 165 of an actual reconnection ‘exhaust’ if the  $\Delta T_e$  supported that hypothesis; otherwise it is the  
 166 inner edge of a ‘candidate’ exhaust.

167 To determine magnetosheath  $T_e$ , we used two methods: the 3d moment method and  
 168 the 1d moment method. These methods are well documented in Lewis et al. (2008). For  
 169 completeness, a summary of the key equations are given below.

170 The 3d moment method integrates the velocity distribution function  $f(\mathbf{v})$  measured  
 171 by ELS at a given time over the velocity volume. The density ( $n$ ) and temperature ( $T$ )  
 172 moments are calculated as follows:

$$\begin{aligned} n &= \int f(\mathbf{v})d^3\mathbf{v} \\ T &= \frac{m}{3nk_B} \int v^2 f(\mathbf{v})d^3\mathbf{v} \end{aligned} \quad (2)$$

173 where  $k_B$  is the Boltzmann constant and  $m$  is the particle mass. The temperature  
 174 equation uses the average kinetic energy per particle due to thermal motion in three degrees  
 175 of freedom  $m\langle v^2 \rangle/2 = 3k_B T/2$  and  $\langle v^2 \rangle = 1/n \int v^2 f(\mathbf{v})d^3\mathbf{v}$ , under the assumptions of a  
 176 Maxwellian distribution and zero bulk flow. Arridge et al. (2009) showed that the bulk  
 177 kinetic energy is always more than 100 times smaller than the typical peak electron energy  
 178 ( $\sim 100$  eV), thus justifying the zero bulk velocity assumption. For ions, the bulk flow cannot  
 179 be neglected and  $v \rightarrow (\mathbf{v} - \mathbf{v}_b)$  where  $\mathbf{v}_b$  is the bulk flow velocity. Under the assumptions of  
 180 an isotropic  $f(\mathbf{v})$  for the electrons ( $d^3\mathbf{v} \rightarrow 4\pi v^2 dv$ ), and a constant  $f(\mathbf{v})$  across each energy  
 181 bin, the integrals in equation 2 become a sum over 63 energy bins in ELS:

$$\begin{aligned} n &= \frac{4\pi}{3} \sum_{i=1}^{i=63} f(v_{i,m})(v_i^3 - v_{i-1}^3) \\ T &= \frac{4\pi m}{15nk_B} \sum_{i=1}^{i=63} f(v_{i,m})(v_i^5 - v_{i-1}^5) \end{aligned} \quad (3)$$

182 where subscripts  $i, i - 1$  represent the upper and lower boundary of the  $i^{th}$  energy  
 183 bin, and  $v_{i,m} = \sqrt{2E_{i,m}/m}$  (where  $E_{i,m}$  is the centroid energy of each bin ranging from

184 0.58 eV to 26 keV) (Lewis et al., 2008). Each term of these summations makes a finite  
 185 contribution to the total density and temperature. However, as the magnetopause boundary  
 186 is an intermediate region between the magnetosheath and magnetosphere, the plasma in this  
 187 region is likely a mixed population of magnetosheath and magnetospheric plasmas. We used  
 188 a cut-off of 150 eV for delineating two electron populations (cold, < 150 eV, and hot, > 150  
 189 eV). This cut-off is  $\sim 3$  times the modal energy of magnetosheath electrons (typically  $\sim$   
 190 50 eV, see for example the peak of the energy distribution in Figure 2a). This is high  
 191 enough to capture the low energy magnetosheath population, but not so high as to include  
 192 hotter magnetospheric electrons in the plasma. In this study, we determine both the full  
 193 temperature by summing over all the energy bins and the ‘cold population’ temperature by  
 194 summing only bins below 150 eV (bin index  $i = 30$ ).

195 The 1d moment method assumes that the energy distribution function is Maxwellian,  
 196 given by:

$$f_{\text{Maxwell}}(E) = n \left( \frac{m}{2\pi k_B T} \right)^{3/2} \exp \left( \frac{-E}{k_B T} \right). \quad (4)$$

197 In the 1d method, a Gaussian of the form

$$g(E) = A_0 \exp \left( \frac{-(E - A_1)^2}{2A_2^2} \right). \quad (5)$$

198 where  $A_0$ ,  $A_1$ ,  $A_2$  are the, height, mean value and standard deviation of the Gaussian  
 199 respectively, is fitted to the electron counts per second data (or count rate  $R_c$ ) against  
 200 energy ( $E$ ) at a given time from the ELS instrument to extract the energy that maximises  
 201 the count rate (i.e. where the derivative  $dR_c/dE = 0$ ). The derivative  $dR_c/dE$  is obtained  
 202 by equating the Maxwellian in equation 4 to the phase space density (PSD) derived from  
 203 count rate data using equation 6, and differentiating with respect to energy:

$$f(v) = \frac{2R_c}{v^4 G(E)}, \quad (6)$$

204 where  $R_c = N/t_a$  is the electron count rate data based on returned electron counts  $N$   
 205 and accumulation time  $t_a = 23.4\text{ms}$ ; corrected for anode dependent efficiency and then con-  
 206 verted to the corrected counts per second,  $v$  is the velocity associated with the measurement  
 207 energy derived from  $v = \sqrt{2E/m}$ , and  $G(E)$  is the instrument energy-dependent geometric  
 208 factor. By setting  $dR_c/dE = 0$ , the Maxwellian temperature and density parameters are  
 209 found by:

$$\begin{aligned} T &= \frac{A_1}{k_B \left( 2 + \frac{d \ln G}{d \ln E} \right)} \approx \frac{A_1}{2k_B} \\ n &= \left( \frac{\pi}{2} \right)^{\frac{3}{2}} \frac{A_0}{G(A_1)} \sqrt{\frac{m}{k_B T}} \exp(2). \end{aligned} \quad (7)$$

where  $A_1$  is the estimated peak energy and  $A_0$  is the estimated peak count rate from the Gaussian fit. A corresponding Maxwellian is derived by inserting  $n$  and  $T$  into equation 4. We refer the reader to Lewis et al. (2008) for a detailed derivation.

A Kappa distribution (Pierrard & Lazar, 2010) of the following form can also be fitted to the PSD data:

$$f_{\text{Kappa}}(v) = \frac{n}{(\pi\kappa w^2)^{\frac{3}{2}}} \frac{\Gamma(\kappa + 1)}{\Gamma(\kappa - 1/2)} \left(1 + \frac{v^2}{\kappa w^2}\right)^{-(\kappa+1)}, \quad (8)$$

where  $w = \sqrt{(2\kappa - 3)k_B T / \kappa m}$  is the most probable thermal velocity,  $n$  is the number density,  $\Gamma(x)$  is the Gamma function,  $\kappa$  is the kappa index which determines the slope of the energy spectrum in the high energy tail, and  $T$  is the equivalent temperature of the plasma such that  $3k_B T / 2$  represents the mean energy per particle of the distribution. The full 3d temperature and density moments can be used as plasma parameters in this distribution to fit to observations with a high-energy tail; a low  $\kappa$  value indicates substantive suprathermal tail whilst a high value indicates a distribution close to Maxwellian (i.e. the Maxwellian distribution is a special case of the more general kappa distribution). In the limit  $\kappa \rightarrow \infty$ ,  $w = \sqrt{2k_B T / m}$  becomes the most probable speed of a Maxwellian. The kappa index must be larger than the critical value  $\kappa_c = 3/2$ , where the distribution function collapses and the temperature is not defined.

An example of the fitted curves and corresponding data is shown in Figure 2. Three different routines were used to fit the Gaussian, namely: ‘polyfit cut’, ‘polyfit weighted’ and ‘nlinfit’:

- In ‘polyfit cut’, the data were truncated at 150eV to remove the influence of the previously defined hot population. A further thresholding was applied to only include points in the fit if their value was greater than 20% of the maximum (keeping points in the vicinity of the peak value). Using the `polyfit` routine in Matlab, a quadratic polynomial fit is performed on the natural log of the count rate data. The natural logarithm transforms Gaussian-like data into a parabola for input into the `polyfit` routine. This is a least squares problem of the form  $Vp = y$ , where  $V$  is a Vandermonde matrix constructed from the energy bin values,  $y$  is the logged count rate data and  $p$  is the least squares solution containing the polynomial coefficients. These coefficients determine the Gaussian parameters  $A_0$ ,  $A_1$  and  $A_2$ .
- In polyfit weighted, an additional weight vector ( $w$ ) is used, modifying the least squares problem to  $Vp = yw$ . Using the normalised root mean squared error (NRMSE) to quantify the closeness of Gaussian fit to the peak of the distribution, the best weight vector of form  $w = y^i$  is found. Generally,  $i = 4$  is found to work well. The weight vector essentially augments the count rate around the peak of the distribution such that a better fit at the peak would preferentially minimise the squared residuals.
- The third method, `nlinfit`, is a nonlinear regression routine in Matlab which uses an iterative Levenberg-Marquardt least squares algorithm to estimate the Gaussian

247 parameters that minimise the squared residuals between the counts data and the  
 248 model, with initial values specified by the `polyfit` routine.

249 The technique which showed the most stable results (i.e. without nonphysical values in the  
 250 fitted Gaussian such as negative temperature) was used in determining the 1d temperature.

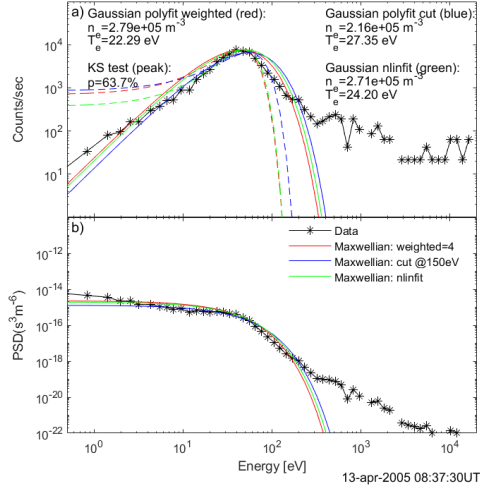


Figure 2: An example of various fitting techniques used in the 1d moment method. The black lines in panel a) and b) are the counts per second data and PSD distribution functions measured by CAPS–ELS on 13 April 2005 at 0837 UT (corrected for photoelectrons). Gaussian curves, fitted using different techniques, shown as dashed lines. Using the density and temperature values derived from the peak of the Gaussian, the corresponding Maxwellian is derived using equation 4. The Maxwellian curves shown as solid lines are used to perform Kolmogorov–Smirnov (KS) tests against the seven points in the neighbourhood of the peak value. The result of this test for the ‘nlinfit’ Maxwellian is shown on the plot.

251 Fundamentally, heating is due to particles scattered from one region of velocity space  
 252 into another region, increasing the volume in velocity space. Given that the 1d moment  
 253 method restricts to a single Maxwellian population, an increase in the phase space  
 254 density at higher energies would correspond to heating of that population. If the 1d  
 255 derived Maxwellian fits well to the low energy spectra, then the magnetosheath population  
 256 can be well described by a Maxwellian distribution. Furthermore, if the 1d plasma  
 257 parameters are in close agreement with the 3d moments, then we can infer that the  
 258 temperature and density moments of the entire distribution can be interpreted as  
 259 Maxwellian plasma parameters of the dominant magnetosheath population. This is key  
 260 for reliably determining the amount of heating caused by reconnection, rather than  
 261 measuring the heating simply due to the additional presence of hotter magnetospheric  
 electrons in the plasma.

262 After obtaining the observed heating  $\Delta T_e$  for each event, we compared it with the  
 263 theoretical value. The semi-empirical formula for electron bulk heating caused by magnetic  
 264 reconnection is (Phan et al., 2013):

$$\Delta T_e = 0.017 m_i V_{AL,in}^2 = 0.017 \frac{B_{L,in}^2}{\mu_0 n_{in}}, \quad (9)$$

265 where  $V_{AL,in}$  is the inflow Alfvén speed based on the inflow reconnecting field  $B_{L,in}$   
 266 and number density  $n_{in}$ . Note that the expression is mass-independent. The constant  
 267 0.017 represents the fraction of inflow magnetic energy per proton-electron pair converted  
 268 to heat. If a MP crossing lies in the ‘reconnection possible’ regime in the  $|\Delta\beta|$ -magnetic  
 269 shear parameter space and the observed heating agrees with prediction within error then  
 270 it is a good indicator that the spacecraft passed through an actual reconnection exhaust  
 271 emanating from a reconnection site local to the spacecraft. Performing minimum variance  
 272 analysis (MVA) (Sonnerup & Scheible, 1998) on the magnetic field data in the MP crossing  
 273 interval yielded the maximum variance direction which determines the reconnecting field  
 274 component ( $B_L$ ). The energy stored in this field component is released during reconnection  
 275 and converted to particle energy (see equation 9). MVA also provides the minimum variance  
 276 direction which is the normal component of the magnetic field  $B_N$  relative to the MP surface.  
 277 We compared the single-sample MVA with the bootstrap MVA method. The main difference  
 278 between the two methods was that the bootstrap method performed a large number of  
 279 minimum variance calculations using bootstrap data samples of the set of magnetic vectors  
 280 in the MP interval of interest (Sonnerup & Scheible, 1998). This produced a set of minimum  
 281 variance eigenvectors and corresponding normal field components  $\{B_N\}$ . The average and  
 282 standard deviation of this set were obtained and found to be close to the  $B_N$  value derived  
 283 from the single-sample method which performs the minimum variance calculation once on  
 284 the same interval of magnetic vectors, with analytical estimates of uncertainty typically of  
 285 order 0.1 nT (Sonnerup & Scheible, 1998). The single-sample MVA was employed in this  
 286 study. The obtained  $B_N$  value and its uncertainty are used to determine whether the MP  
 287 boundary is ‘open’ or ‘closed’.

288 Furthermore, the 70 events were put into three categories:

- 289 1. Steady transitions with field rotation (i.e. polarity change).
- 290 2. Turbulent transitions with field rotation.
- 291 3. Transitions without significant field rotation (i.e. no polarity change).

292 Each event was also labelled by energisation being 0 or 1, where energisation of 1 means the  
 293 heating values calculated from both the 1d and 3d methods for the cold population were  
 294  $>1.5$  eV, with uncertainty typically of the order of 1 eV; otherwise the event was labelled  
 295 energisation of 0.

296 Three case studies of magnetopause crossings are presented to illustrate the character-  
 297 isation and varying amount of electron heating for each category of events. The locations  
 298 of these exemplar crossings in the equatorial plane are shown as stars in Figure 3.

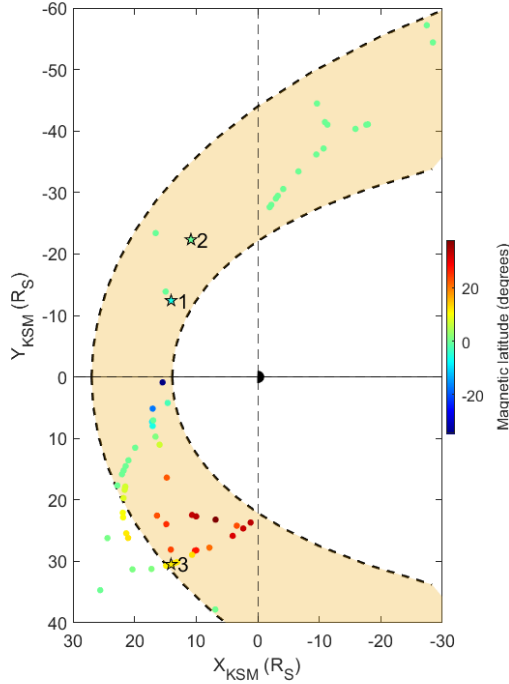


Figure 3: Positions of the 70 Cassini magnetopause crossings made between April 2005 to July 2007 projected onto the XY plane in Kronocentric Solar Magnetospheric (KSM) coordinates with determined full plasma  $\beta$  in both the magnetosheath and magnetosphere (Masters et al., 2012). The colour of the markers indicates magnetic latitude (i.e. with respect to Saturn’s equatorial plane). The dashed black curves give extreme positions of Saturn’s magnetopause at standoff distance  $14R_S$  and  $27R_S$  based on model in Pilkington et al. (2015). The crossing positions shown as a star with labels 1, 2 and 3 correspond to the three case studies.

### 3.1 Case Study 1: Steady Magnetopause Crossing With Field Rotation and substantial Electron Bulk Heating

Figure 4 shows an inbound magnetopause crossing by Cassini at low magnetic latitude ( $-6.44^\circ$ ) in the pre-noon sector (9:20 LT) at a radial distance of  $19R_S$  ( $1R_S = 60268$  km is Saturn’s equatorial radius). The crossing duration was  $\sim 9.5$  minutes. The magnetic shear across the MP was  $\sim 93 \pm 4^\circ$ , based on the dot product of the average fields in the intervals marked by the two pairs of dashed lines in Figure 4 either side of the MP. The eigenvalue ratio of the intermediate and minimum variance direction was  $\lambda_2/\lambda_3 = 13$ . As a rule of thumb, a well-defined boundary transition has  $\lambda_2/\lambda_3 \approx 10$  (Sonnerup & Scheible, 1998). The ratio of the average normal component of the magnetic field compared with the average total field in the magnetopause is  $B_N/B = 0.015 \pm 0.026$ . This value is negligible within the error and indicates that the boundary may have been locally closed, forming a

311 tangential discontinuity (TD). The magnetosheath and magnetospheric full plasma  $\beta$  were  
 312  $\sim 1.0$  and  $\sim 1.5$  respectively, leading to a change of  $\Delta\beta \approx 0.5$ . The ion Alfvén speed based  
 313 on the reconnecting field ( $B_L$ ) was  $386 \pm 1$  km/s. This event was an exemplar of category 1  
 314 due to the steady crossing conditions as shown by a well defined red band of magnetosheath  
 315 electrons in the spectrogram and clear transition in moments aligned with a polarity change  
 316 in the  $B_L$  magnetic field component either side of the magnetopause. We describe the event  
 317 from left to right going from the magnetosheath to the magnetosphere as we investigate the  
 318 heating of the entering magnetosheath electrons.

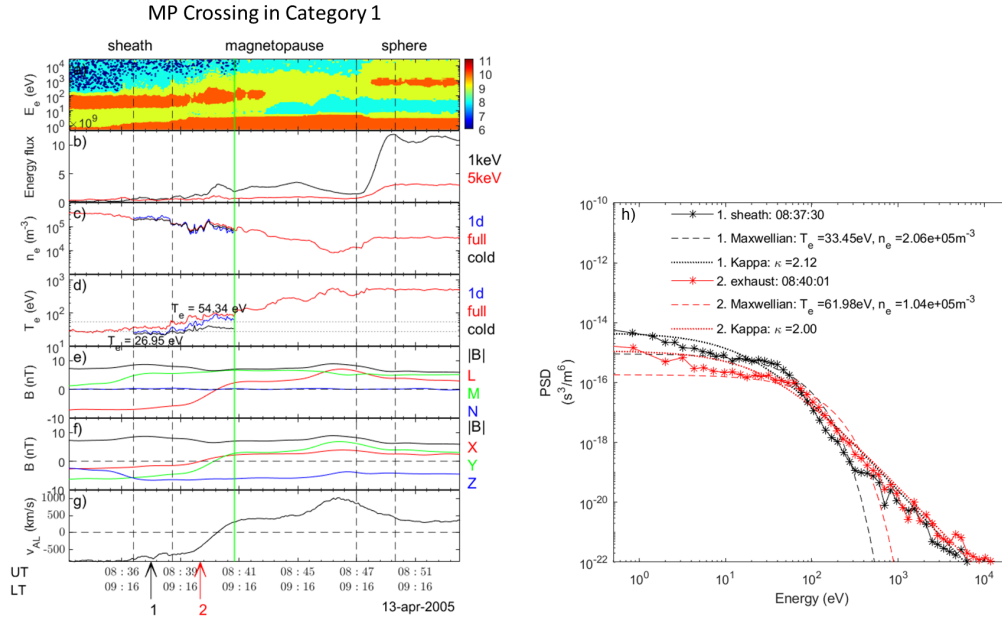


Figure 4: Exemplar magnetopause crossing with evidence of electron heating in category 1: Steady transition with field rotation. The panels are (a) Energy-time spectrogram of decimal logarithm of electron Differential Energy Flux (DEF) ( $eVs^{-1}m^{-2}ster^{-1}eV^{-1}$ ) from ELS anode 5. The red band below  $\sim 5$  eV is spacecraft photoelectrons. (b) DEF of 1 keV and 5 keV electrons. (c,d) Electron number density ( $m^{-3}$ ) and temperature ( $eV$ ) based on the 3d moment methods (full, cold) and 1d moment method (1d). (e) Magnetic field in minimum variance coordinates. (f) Magnetic field in KSM Coordinates. (g) Alfvén speed based on  $B_L$  and proton mass density. (h) Electron spectra in the magnetosheath (black) and in the exhaust (red) corrected for photoelectrons using the spacecraft potential, with overlaid Maxwellian distributions, and fitted Kappa distributions, using measured density and temperature moments (full) as the plasma parameters. Labels ‘1’ and ‘2’ under panel g point to the times of the cuts shown in panel h. The pairs of dashed black vertical lines immediately before and after the MP crossing denote the magnetosheath and magnetospheric intervals that define the boundary conditions of the magnetopause current layer. The green vertical line denotes the innermost location of the magnetosheath boundary layer for the computation of the average electron temperature in this region.

319 Across the magnetosheath boundary layer (‘exhaust’), the 1d temperature of the thermal  
 320 population (containing most of the electrons) increased gradually, from  $\sim 27 \pm 1$  eV  
 321 (in the pristine magnetosheath) to  $\sim 54 \pm 3$  eV in the exhaust (blue line in Figure 4d),  
 322 where the uncertainty is the standard error of the mean temperature in each region. The  
 323 temperature increased even further deeper within the magnetopause. Thus, the average  
 324 amount of magnetosheath electron heating for this event was  $\Delta T_{e,obs} = 27 \pm 2.6$  eV. The  
 325 predicted heating due to reconnection using equation 9 was  $\Delta T_{e,pred} = 26.5 \pm 0.2$  eV which  
 326 is in good agreement with the observation within uncertainty. The heating of the entering  
 327 magnetosheath electrons is also evident in the electron energy-time spectrogram (Figure  
 328 4a), which shows an upward energy shift of the red band at the beginning of the exhaust.  
 329 Since the 1D temperature depends on just the peak energy, a depletion in low energy elec-  
 330 trons for example should not affect the temperature value and we can assume the measured  
 331 heating is due to magnetosheath electrons being shifted to higher energy. Figure 4h shows  
 332 representative electron PSD distributions in the magnetosheath (black) and in the exhaust  
 333 (red); the overlaid Maxwellian dashed curves correspond to the density and temperature  
 334 derived from the entire electron energy distribution corrected from the spacecraft potential  
 335 to exclude the contributions of photoelectrons (Lewis et al., 2008). The observed phase  
 336 space density (PSD) in the magnetosheath fits marginally well to a Maxwellian between  
 337 energies 10 to 300 eV but deviates significantly outside this range. For the exhaust, the  
 338 PSD significantly deviates from Maxwellian beyond  $\sim 500$  eV. The root mean square error  
 339  $RMSE = \sqrt{\sum(y_{obs} - y_{pred})^2/N}$  is used as a measure of the accuracy of the fit, where N is  
 340 the number of points. A larger value indicates less accurate fit. Between 10 eV and 150 eV,  
 341 the RMSE of the magnetosheath and exhaust regions were  $0.73 \times 10^{-16}$  and  $0.34 \times 10^{-16}$   
 342 respectively. As a comparison for the whole energy range, the RMSE were  $0.12 \times 10^{-14}$   
 343 and  $0.03 \times 10^{-14}$  respectively, two orders of magnitude larger. This indicates that the tem-  
 344 perature in this event is dominated by the core electrons of magnetosheath origin, with  
 345 suprathermal (‘hot’) electrons contributing noticeably to the overall temperature (for ex-  
 346 ample, compare the red and blue lines in the exhaust region of Figure 4d).

347 A kappa distribution with  $\kappa$  fitted to the observed distributions using the full tem-  
 348 perature and density moments, yielding  $\kappa$  of 2.12 and 2.00 for the magnetosheath and  
 349 exhaust respectively. The kappa distribution is able to describe well the slow drop-off of  
 350 the high-energy tail in the PSD ( $>300$  eV in the magnetosheath and  $>500$  eV in the ex-  
 351 haust), indicating that the sampled population is a mixture of the magnetosheath and the  
 352 magnetospheric populations. The kappa fits give RMSE of  $0.62 \times 10^{-15}$  and  $0.19 \times 10^{-15}$  re-  
 353 spectively for the whole energy range, an order of magnitude smaller than single Maxwellian  
 354 indicating a better fit. The fact that suprathermal electrons can contribute substantially to  
 355 the temperature moment makes the full 3d temperature method unreliable for calculating  
 356 heating as the value could be falsely augmented by the mixing of a magnetospheric hot  
 357 population in the exhaust. Thus, the electron heating in all the events was calculated using  
 358 the 1d method which assumes that the core electrons (i.e. energies encompassing the most  
 359 electrons) form a single Maxwellian population.

Figure 2a shows the 1d temperature and density plasma parameter at 08:37:30 UT (label ‘1’ in Figure 4g) derived from the Gaussian fits. The corresponding Maxwellian curves showed good fit around the peak of the data. The densities are similar between all three fitting techniques and in good agreement with the 3d density moments shown in Figure 4h. This means that the core electron population accounts for most of the electrons in this region. There is satisfactory agreement in temperature between the 1d and 3d values, although 1d values are lower as it does not include the high energy tail in the data. Thus, although the hot population contributes little to the density, it may contribute a significant amount to the temperature moments. The Maxwellians (solid lines) were used to perform KS tests against the ELS counts of seven points around the peak. The obtained p-value of 63.7% is the probability of observing a test statistic, as extreme as, or more extreme than the observed value under the null hypothesis. Since the p-value is large, we cannot (at this level of  $p$ ) reject the null hypothesis that the peak of the distribution is Maxwellian.

Figure 4b shows that the fluxes of 1 keV and 5 keV electrons (mostly of magnetospheric origin) were very low in the magnetosheath. A small increase is observed at  $\sim$ 08:40 UT but remained fairly constant throughout the magnetopause until the magnetospheric edge of the magnetopause, at  $\sim$ 08:47 UT, where these fluxes increased sharply. Thus, to study the amount of magnetosheath electron heating that occurred, we only consider the interval from the magnetosheath edge of the magnetopause to the location just before the magnetospheric electrons first appear (at  $\sim$  08:39:54 UT, marked by the green vertical line) in order to minimise contamination from the magnetospheric plasma. The location where magnetospheric electrons first appear also marks the location where the density begins to drop monotonically and more rapidly. However, it was apparent that many events did not show a clear increase in the fluxes of 1 keV and 5 keV electrons (see section 3.2). For those cases, the abrupt dip in the density profile was used to determine the inner edge of the exhaust.

This event appears to have a locally closed boundary, yet temperature change was observed in magnetosheath electrons consistent with prediction, in contrary to hypothesis 1. We suggest that it may be due to detecting heated electrons from a remote magnetically conjugate reconnection site at the magnetopause with similar plasma and field conditions. A magnetic shear of  $\sim 93^\circ$  and  $\Delta\beta \approx 0.5$  places this event in the ‘reconnection possible’ regime, consistent with hypothesis 2, since evidence of plasma energisation was also observed.

### 3.2 Case Study 2: Turbulent Magnetopause Crossing With Field Rotation and Electron Bulk Heating

Figure 5 shows an inbound magnetopause crossing by Cassini at low magnetic latitude ( $-0.29^\circ$ ) near dawn (7:47 LT) at a range of  $25R_S$ . The crossing duration was  $\sim 17$  minutes. The magnetic shear across the magnetopause was  $\sim 88.9 \pm 3^\circ$ . The eigenvalue ratio of the intermediate and minimum variance magnetic field direction is  $\lambda_2/\lambda_3 = 2.55$ ; this small value suggests a less reliable normal direction was obtained. The ratio of the average normal component of the magnetic field compared with the average total field in the MPCL is

400  $B_N/B = 0.19 \pm 0.08$ . This value is marginally non-zero, given the uncertainty, which suggests  
 401 that the magnetopause could be magnetically open, forming a rotational discontinuity (RD).  
 402 The magnetosheath and magnetospheric full plasma  $\beta$  were  $\sim 1.6$  and  $\sim 0.5$  respectively,  
 403 leading to a change of  $\Delta\beta \approx 1.1$ . The ion Alfvén speed based on the reconnecting field ( $B_L$ )  
 404 was  $358 \pm 2$  km/s. This event is in category 2 due to more turbulent crossing conditions  
 405 as seen in the patchy spectrogram with intermittent energisation of the magnetosheath  
 406 electrons and also breaks in the red band, likely due to mixing between magnetosheath and  
 407 magnetospheric populations. However, there is still a clear polarity change in the  $B_L$  field  
 408 either side of the MP.

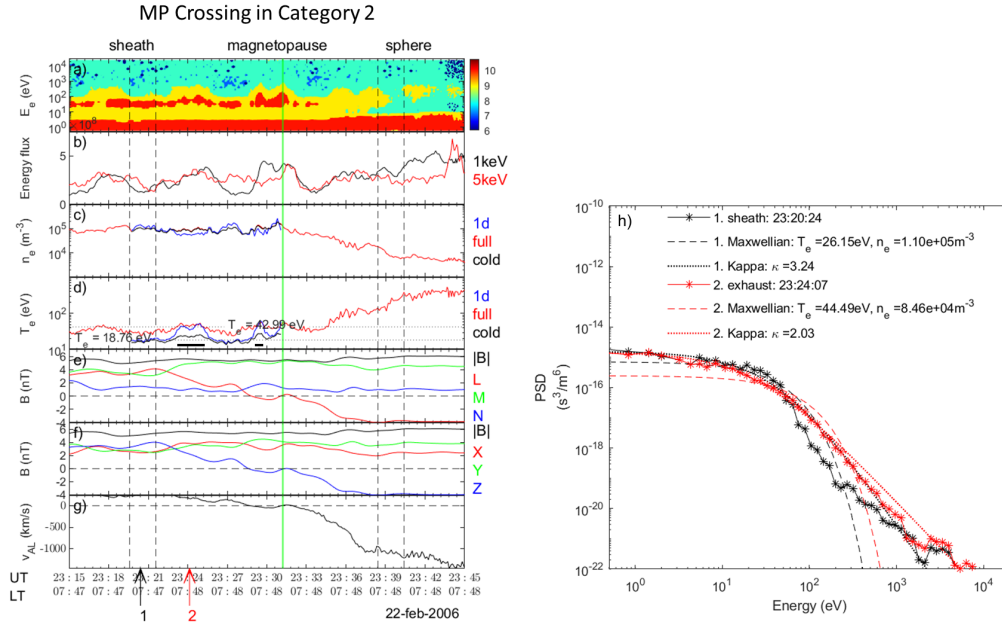


Figure 5: Exemplar magnetopause crossing with evidence of electron heating in category 2: Turbulent transition with field rotation. The format of the panels is identical to Figure 4.

409 In contrast to Case Study 1, the intermittent energisation in this event caused an  
 410 underestimation of the heating if we simply consider the average temperature in the entire  
 411 exhaust (between the second dashed black line on the left and the green solid line in Figure  
 412 5). To mitigate this effect, the average temperature of only the heated electrons was used.  
 413 This corresponded to time intervals of 23:23:24 to 23:25:12 UT and 23:28:48 to 23:29:24 UT  
 414 (marked by horizontal bars in Figure 5d). Thus, the average amount of electron heating  
 415 for this event was  $\Delta T_{e,obs} = 24.2 \pm 1.5$  eV. The predicted heating due to reconnection  
 416 was  $\Delta T_{e,pred} = 22.8 \pm 0.3$  eV which is in good agreement with the observation within  
 417 the uncertainty. Figure 5h shows that the exhaust PSD is clearly higher than than the  
 418 magnetosheath PSD around the 100 eV region, also indicative of heating.

419 The rotation from northward external field to southward planetary field, together with  
 420 moderate value for magnetic shear offers ideal condition for local reconnection, consistent  
 421 with the fact that the electrons of magnetosheath origin were clearly hotter in parts of  
 422 this field rotation than in the adjacent pristine magnetosheath, and that the magnetopause  
 423 appeared to be locally open. These observations are consistent with hypothesis 1 that locally  
 424 open magnetopause should have observed  $\Delta T_e$  close to theoretical prediction. A magnetic  
 425 shear of  $\sim 88.9^\circ$  and  $\Delta\beta \approx 1.1$  places this event in the ‘reconnection possible’ regime,  
 426 consistent with hypothesis 2 that evidence of plasma energisation was observed.

### 427 **3.3 Case Study 3: Magnetopause Crossing Without Field Rotation and** 428 **Insignificant Electron Bulk Heating**

429 Figure 6 shows an outbound magnetopause crossing by Cassini at low magnetic latitude  
 430 ( $11.6^\circ$ ) near dusk at Saturn (16:09 LT) at a range of  $35R_S$ . The crossing duration was  $\sim 8.4$   
 431 minutes. The magnetic shear across the magnetopause was low,  $\sim 32 \pm 23^\circ$ . The eigenvalue  
 432 ratio of the intermediate and minimum variance direction is  $\lambda_2/\lambda_3 = 2.20$ , even smaller  
 433 than in Case Study 2 and consistent with near-parallel magnetospheric and magnetosheath  
 434 fields. The ratio of the average normal component of the magnetic field compared with the  
 435 average total field in the MP layer is  $B_N/B = 0.46 \pm 0.03$ . Although this suggests an open  
 436 magnetopause it is an unreliable value due to the small separation between the minimum  
 437 and intermediate eigenvalues. In such cases, it may be necessary to impose a constraint  
 438  $\langle \mathbf{B} \rangle \cdot \hat{\mathbf{n}} = 0$  (i.e.  $B_N/B = 0$  and boundary is closed) for MVA to obtain a useful normal  
 439 vector prediction (Sonnerup & Scheible, 1998). The magnetosheath and magnetospheric  
 440 full plasma beta were  $\sim 11.24$  and  $\sim 8.06$  respectively, leading to a change of  $\Delta\beta \approx 3.17$ ,  
 441 higher compared to case studies 1 and 2. The ion Alfvén speed based on the reconnecting  
 442 field ( $B_L$ ) was  $121 \pm 1$  km/s. This event is in category 3 as there was no polarity change  
 443 in the maximum variance component of the magnetic field ( $B_L$ ) either side of the MP. We  
 444 describe this event from right (magnetosheath) to left (magnetosphere).

445 In contrast to Case Study 1 and 2, the electron temperature did not increase in the  
 446 exhaust and remained roughly constant until 15:55:12 UT when hot ( $> 1$  keV) magne-  
 447 to-spheric electrons began to appear and density dropped monotonically (Figure 6b and 6c).  
 448 The absence of bulk heating of entering magnetosheath electrons is also clear in the elec-  
 449 tron spectrogram, which shows essentially no variations across the MP. Similarly, Figure  
 450 6h shows that the electron spectra in the magnetosheath (black curve) and in the magne-  
 451 tosheath side of the magnetopause (red curve) were nearly identical. The average amount  
 452 of bulk temperature change for this event was only  $\Delta T_{e,obs} \approx 1.12 \pm 0.57$  eV. The predicted  
 453 heating due to reconnection was  $\Delta T_{e,pred} = 2.59 \pm 0.02$  eV. The discrepancy suggests that  
 454 the conditions measured by the spacecraft may be quite different to those at any putative  
 455 reconnection site. Furthermore, the small predicted value suggests that local conditions are  
 456 not viable for reconnection. In such a case, in the absence of other evidence, one concludes  
 457 that this is most likely a case of a closed magnetopause with no active reconnection. This  
 458 conclusion would be consistent with hypothesis 1. A magnetic shear of  $\sim 32^\circ$  and  $\Delta\beta \approx 3.17$   
 459 places this event in the ‘reconnection suppressed’ regime, consistent with hypothesis 2 that

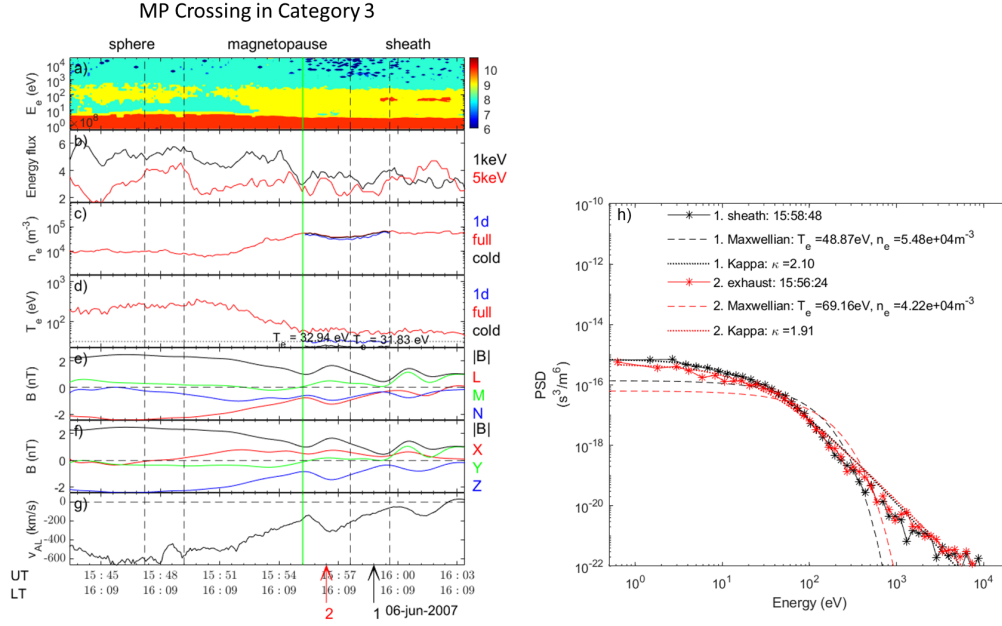


Figure 6: Exemplar magnetopause crossing without evidence of electron heating in category 3: Transitions without significant field rotation. The format of the panels is identical to Figure 4.

460 no significant energisation was observed (nominal value of  $\Delta T_{e,obs}$  is less than twice its  
 461 uncertainty).

462 The key parameters responsible for the differences in bulk electron heating in these  
 463 events are the change in plasma beta ( $\Delta\beta$ ) across the magnetopause, magnetic shear, and  
 464 the Alfvén speed. The purpose of the statistical survey is to reveal whether there is a  
 465 correlation between the agreement of observed and predicted heating and the parameters  
 466 that play a role in the viability of reconnection at Saturn’s magnetopause, as detailed in  
 467 Masters et al. (2012).

## 4 Results

A statistical overview of the 70 events is provided below. One event had unclear boundary crossing in both field and plasma parameters and was omitted from the analysis. We found 45 (66%), 12 (17%) and 12 (17%) events in categories 1, 2 and 3 respectively. 39 (57%) events have an open MP based on the criteria of  $B_N/B \geq 0.1$ . 28 (41%) events showed evidence of energisation based on temperature change threshold of  $\Delta T_e > 1.5\text{eV}$  after accounting for uncertainty. In all three methods of calculating heating, we find a few events with negative temperature change moving from pristine magnetosheath to magnetosheath edge of the MP, the largest being almost  $-5\text{ eV}$  based on the 1d temperatures. Note that the typical standard error of the mean temperature in each region is  $\sim 1\text{ eV}$ . There are also intrinsic errors at the source of measurements associated with the ELS sensor, such as Poisson counting statistical uncertainty and the assumption of isotropic distribution function as CAPS had limited angular coverage. Arridge et al. (2009) showed temperature uncertainty is less than 20% above a temperature of 10 eV which would lead to a temperature change between the two regions to be consistent with zero for these negative cases. On the other hand, if these cooling effects were real, it could be that the MP boundary is often not static due to varying pressures from external solar wind and internal plasma loading. The movement of the MP could change the thickness of the magnetosheath leading to expanded flux tubes which undergo adiabatic cooling. This must remain a speculative statement until future related analysis takes place.

Plots of observed versus predicted electron temperature change for all 70 crossings using the three methods of temperature determination are shown in Figure 7. The events were subdivided into two groups based on their ratio of the normal component of the magnetic field (i.e. minimum variance component) compared with the average field strength in the magnetopause layer. A non-zero ratio within the error indicates an open magnetopause which could be an indicator of recent or ongoing reconnection local to the spacecraft. A ratio of  $B_N/B = 0.1$  was used as a cutoff between ‘open’ and ‘closed’ boundary based on the assumption that, at a reconnecting magnetopause, we may assume that the field and particle velocities follow this relationship:  $B_N/B = v_n/v_A = M_A$ , where  $M_A$  is the Alfvén-Mach number (Sonnerup et al., 1981). At Earth, this ratio is roughly 0.1 (Sonnerup et al., 1981) but reconnection signatures at Saturn’s MP have been observed with  $B_N/B = 0.04$  (McAndrews et al., 2008), indicating slower reconnection process than typically found at Earth. To assess how well the observed temperature changes match the semi-empirical predictions, a linear model is fitted to all 70 data points using weighted least squares method (from `statsmodels` module in Python) with intercept set to zero (not shown). The weight value is inversely proportional to the squared error. The reason for dropping the intercept is due to equation 9 which says that the presence of electron heating requires non-zero Alfvén speed, thus there should be no constant offset.

For the 3d moment method based on the full observed energy distribution (left panels), the observations show little correlation to the prediction (assuming local reconnection). The regression performed on all data points gives a  $r^2$  (or coefficient of determination) of 0.11 and

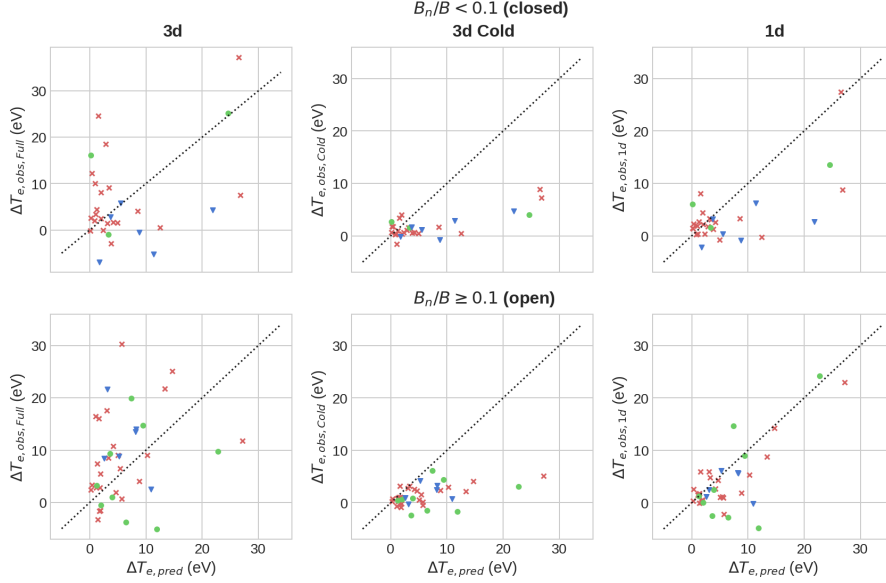


Figure 7: Observed against predicted bulk electron temperature change for all the crossings. Left: Heating based on 3d moment method for full energy distribution. Middle: Heating based on 3d moment method for the cold energy distribution ( $< 150\text{eV}$ ). Right: Heating based on 1d moment method for the peak of the energy distribution. Top panels represent locally ‘closed’ boundary based on threshold  $B_N/B < 0.1$ . Bottom panels represent locally ‘open’ boundary based on threshold  $B_N/B \geq 0.1$ . Red ‘x’ markers: Steady transitions with field rotation (category 1). Green ‘o’ markers: Turbulent transitions with field rotation (category 2). Blue ‘v’ markers: Transitions without significant field rotation (category 3). The dotted line represents agreement between observed and predicted  $\Delta T_e$  (assuming local reconnection).

509 a slope of  $1.18 \pm 0.42$ . The  $r^2$  value quantifies the proportion of the variance in the dependent  
 510 variable ( $\Delta T_{e,obs}$ ) that is predictable from the independent variables ( $\Delta T_{e,pred}$ ). The low  
 511  $r^2$  obtained clearly highlights the poor agreement between the observations and predictions.  
 512 The slope being greater than unity indicates that using the temperature derived from the  
 513 entire electron energy distribution tend to overestimate the temperature change due to the  
 514 contamination from the hotter magnetospheric electrons. Thus, this method is unreliable in  
 515 determining bulk temperature change due to reconnection for the magnetosheath electrons.

516 Considering the 3d moment method applied to the cold ( $< 150\text{ eV}$ ) part of the observed  
 517 energy distribution (middle panels), the results show a much tighter spread with positive  
 518 correlation and almost all observations are below predictions. The regression gives  $r^2$  of  
 519  $0.20$  and a slope of  $0.60 \pm 0.15$ . Note that this method produces systematically lower  
 520 temperature changes as the summation in phase space density up to  $150\text{ eV}$  implies no  
 521 electrons at energies above  $150\text{ eV}$  for the core population which is not the case.

522 Electron heating calculated using the 1d method (right panels) show a clear positive  
 523 correlation between the observation and prediction. The regression slope was  $0.66 \pm 0.01$ ,  
 524 an  $r^2$  of 0.99, and a p-value less than 0.001. The residual plot of the linear fit shows  
 525 random distribution around zero. This result is suggestive of energisation comparable to  
 526 that associated with the reconnection process, albeit weaker than prediction on average.  
 527 With regards to hypothesis 1 that an ‘open’ magnetopause should show signs of heating close  
 528 to prediction, we do see qualitatively a tendency of better agreement with prediction for the  
 529 locally ‘open’ boundary cases based on the threshold  $B_N/B \geq 0.1$  for the minimum variance  
 530 component of the magnetic field. For the case of locally ‘closed’ boundary ( $B_N/B < 0.1$ ),  
 531 we observe qualitatively a cluster of points near  $\Delta T_e \sim 0$ , but also numerous cases of  
 532 significant heating far from prediction. We find five cases where the observed heating exceeds  
 533 prediction significantly ( $>3\text{eV}$ ) with typical uncertainties of the order of 1 eV. These results  
 534 suggest that although the majority of events fit our hypothesis 1 within the uncertainty, the  
 535 minority of events which do not, may be at a closed magnetopause, connected to a remote  
 536 reconnection site.

537 The Kolmogorov-Smirnov (KS) test was used to test whether the two independent  
 538 samples of electron heating for open and closed MP are drawn same underlying continuous  
 539 population. A two-sided test was used for the alternative hypothesis which states that the  
 540 empirical cumulative distribution function ( $ECDF_1$ ) of sample 1 is less or greater than the  
 541  $ECDF_2$  of sample 2. The KS statistic is found from the maximum deviation between the  
 542 ECDFs of the two samples. If the KS statistic is small or the p-value is high compared  
 543 to a predefined significance level (e.g.  $\alpha = 0.1$ ), then we cannot reject the null hypothesis  
 544 that the two samples are from the same underlying distribution. The KS test assumes  
 545 continuous distributions. We test the ratio  $\Delta T_{e,obs,1d}/\Delta T_{e,pred}$  which acts as a quantitative  
 546 measure of the closeness to the predicted heating; a value of 1 indicates perfect match. The  
 547 mean and standard deviation of this ratio were 3.54 and 7.96 for closed MP, and 0.92 and  
 548 1.47 for open MP, respectively. The p-value obtained from this analysis was 0.56 when all  
 549 events were considered. Neglecting the category 3 (blue ‘v’) events due to very low magnetic  
 550 shear, yielded a p-value of 0.13. The latter result indicates that the null hypothesis could  
 551 be rejected at a significance level of 0.13, indicating that the probability that the heating  
 552 ratio distributions are identical is less than 13%. Performing a Welch’s t-test for the mean  
 553 ratio of two independent samples, which does not assume equal population variance also  
 554 yields a p-value of 0.13. This suggests that open MP heating values are clustered closer  
 555 to their corresponding predicted values than for the case of the closed MP which supports  
 556 hypothesis 1, at a significance level of 0.13.

557 Figure 8 shows the crossings in  $|\Delta\beta|$ -magnetic shear parameter space. Magnetic shears  
 558 are based on average fields either side of the MP. We find 83% of events with no energisation  
 559 were situated in the ‘reconnection suppressed’ regime, and 43% of events with energisation  
 560 lie in the ‘reconnection possible’ regime. This is based on the cutoff marked by the solid  
 561 black line corresponding to a current sheet thickness of one ion inertial length ( $L = d_i$ , see  
 562 Masters et al. (2012) for more detail). These results support hypothesis 2 to some extent.

563 Focusing on the ‘Energisation = 1’ panel (right), we find that there is a cluster of  
 564 six category 3 events at the bottom of the plot with magnetic shear below  $20^\circ$  (i.e. near  
 565 parallel magnetospheric and magnetosheath fields) and all reside in the ‘suppressed’ regime  
 566 despite observational evidence of heated electrons. These events are similar in behaviour  
 567 to ‘Reconnection Event 2’ analysed in McAndrews et al. (2008). Cassini is likely observ-  
 568 ing field lines connected to a distant X-line and measuring energised plasma originating  
 569 from that reconnection site. This can be seen in the simplified diagram (Figure 1) of day  
 570 side magnetopause reconnection, showing a possible spacecraft trajectory where the B-field  
 571 orientation would stay relatively constant throughout the crossing. If we neglected these  
 572 events, 59% of events with energisation lie in the ‘reconnection possible’ regime. Further-  
 573 more, the remaining events in the ‘Reconnection suppressed’ region would lie very close to  
 574 the  $L = 2d_i$  dashed line and may plausibly be included in the ‘reconnection possible’ regime  
 575 given the relatively large uncertainty in  $\Delta\beta$  (see Figure S2 in supporting information of  
 576 Masters et al. (2012)). If we exclude the six ‘outliers’ and use  $L = 2d_i$  as the threshold,  
 577 we now find 68% of events with evidence of energisation lie in the ‘reconnection possible’  
 578 regime. Another interesting observation is that the rest of the events in the energisation =  
 579 1 panel have magnetic shear above  $80^\circ$  suggestive of the high magnetic shear requirement.  
 580 In addition, all the events to the left of the  $L = d_i$  solid line contain the strongest heating  
 581 observed at  $\Delta T_e \geq 20$  eV including Case studies 1 and 2 (see section 3.1, 3.2).

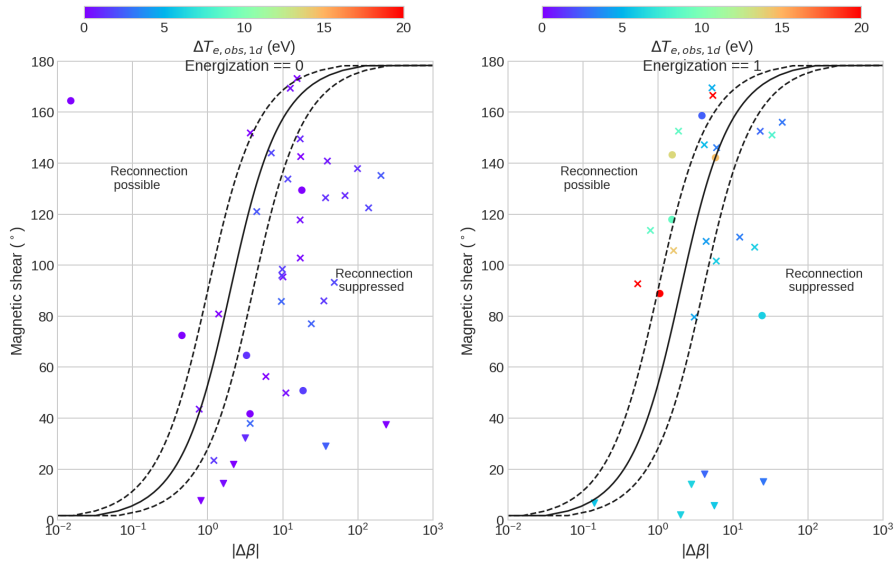


Figure 8: Assessment of diamagnetic suppression of reconnection using the 70 MP crossings. Colour represents observed heating  $\Delta T_e$  using the 1d moment method. The curves are calculated using equation 1, where the solid line corresponds to a current sheet thickness  $L = d_i$ , and the dashed lines on the left and right of it correspond to  $L = 0.5d_i$  and  $L = 2d_i$ , respectively. ‘x’ markers: Steady transitions with field rotation. ‘o’ markers: Turbulent transitions with field rotation. ‘v’ markers: Transitions without significant field rotation.

## 582 5 Conclusions

583 A statistical study of observed and theoretical electron bulk heating was performed at  
 584 the magnetopause based on 70 magnetopause crossings detected by the Cassini spacecraft.  
 585 Our hypotheses were: 1) Closed boundary should have no heating, whilst open boundary  
 586 should have heating close to theoretical prediction (assuming local reconnection). We found  
 587 that the 1d moment method for determining  $T_e$  supports this hypothesis the best, with  
 588 strong correlation between observed and predicted  $\Delta T_e$  for the case of open MP ( $B_N/B \geq$   
 589  $0.1$ ), and a cluster of points near  $\Delta T_e \sim 0$  for the case of closed MP. 2) Events with  
 590 heating should reside in the ‘reconnection possible’ regime and those without should lie  
 591 in the ‘reconnection suppressed’ regime in the  $\Delta\beta$ -magnetic shear parameter space. We  
 592 found 83% of events with no evidence of heating lie in the ‘reconnection suppressed’ regime,  
 593 whilst between 43% to 68% of events with evidence of heating lie in ‘reconnection possible’  
 594 regime depending on the threshold used for current layer thickness. The results of this study  
 595 reinforce the importance of plasma  $\beta$  and magnetic shear across the magnetopause on the  
 596 viability of magnetic reconnection arising at observed locations.

597 One reason why some events do not fit our hypotheses is because we are assuming local  
 598 conditions to be indicative of the putative reconnection site. However, the spacecraft could  
 599 be quite distant from this site, and still magnetically connected to it. With a magnetosphere  
 600 about 20 times larger than Earth’s in absolute size, plasma accelerated by reconnection at  
 601 Saturn may travel a large distance along field lines before reaching the spacecraft. Jasinski  
 602 et al. (2014) showed an example of using the ion energy-pitch angle dispersion (observed  
 603 by the CAPS Ion Mass Spectrometer) to estimate the distance to the reconnection site.  
 604 Their cusp observation of electron energy distributions detected evidence for dayside mag-  
 605 netopause reconnection at a distance of up to  $\sim 51 R_S$  from the reconnection site. Another  
 606 important aspect is temporal variability in the near-magnetopause environment. The combi-  
 607 nation of spatial and temporal variability makes it possible to observe heated electrons with  
 608 different ambient plasma and field conditions from the putative reconnection site, leading to  
 609 discrepancies between theoretical predictions and observations. In addition to these factors,  
 610 the events analysed had relatively weak levels of heating, with only 6 out of 70 events with  
 611 heating stronger than 10 eV, the strongest being around  $\Delta T_e \approx 27$  eV. Some of these heat-  
 612 ing may be caused by mixing of magnetosphere and magnetosheath plasmas, as occurs at  
 613 the MP. Finding events with higher magnetic field strength (e.g. when the magnetosphere  
 614 is strongly compressed with a high magnetosheath field strength) would give faster inflow  
 615 Alfvén speeds, and thus lead to stronger heating giving a reduced relative uncertainty for  
 616 the observed heating. This would provide more data points at higher heating values and  
 617 improve the statistics in comparing between the closed and open magnetopause. A more  
 618 definitive conclusion on the hypotheses requires further analysis. We plan to analyse and  
 619 augment the dataset further in future work utilising recent magnetopause crossings lists  
 620 (e.g. Pilkington et al. (2015); Jackman et al. (2019)), and taking the above aspects into  
 621 consideration.

**Appendix A Plots with error bars**

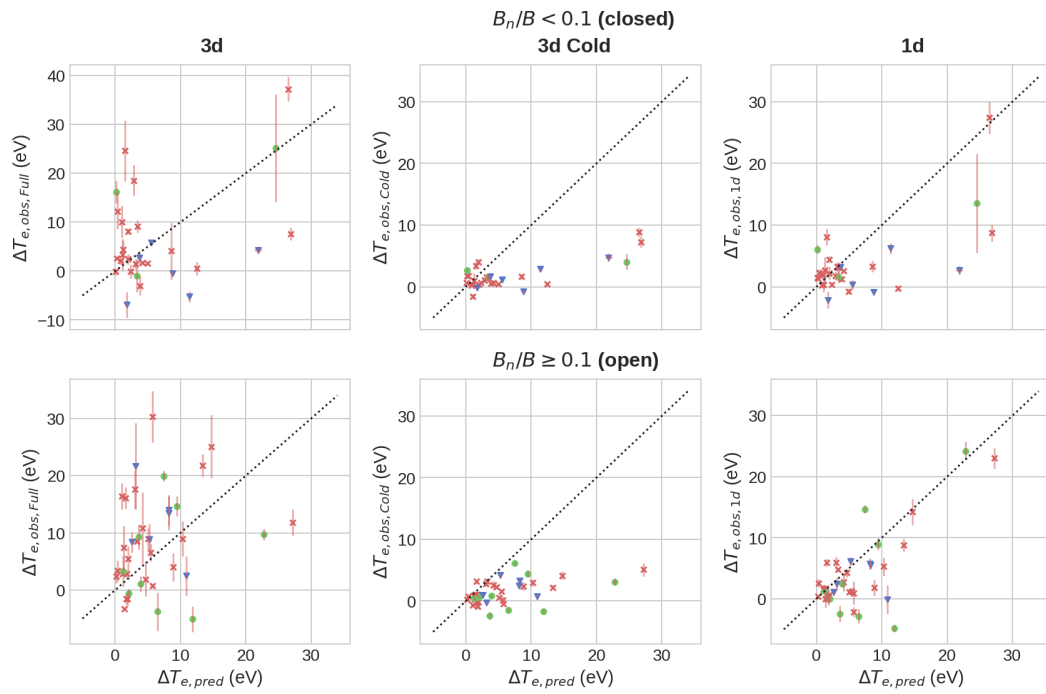


Figure A1: Observed against predicted bulk electron temperature change for all the crossings including results of error analysis. Format is identical to Figure 7.

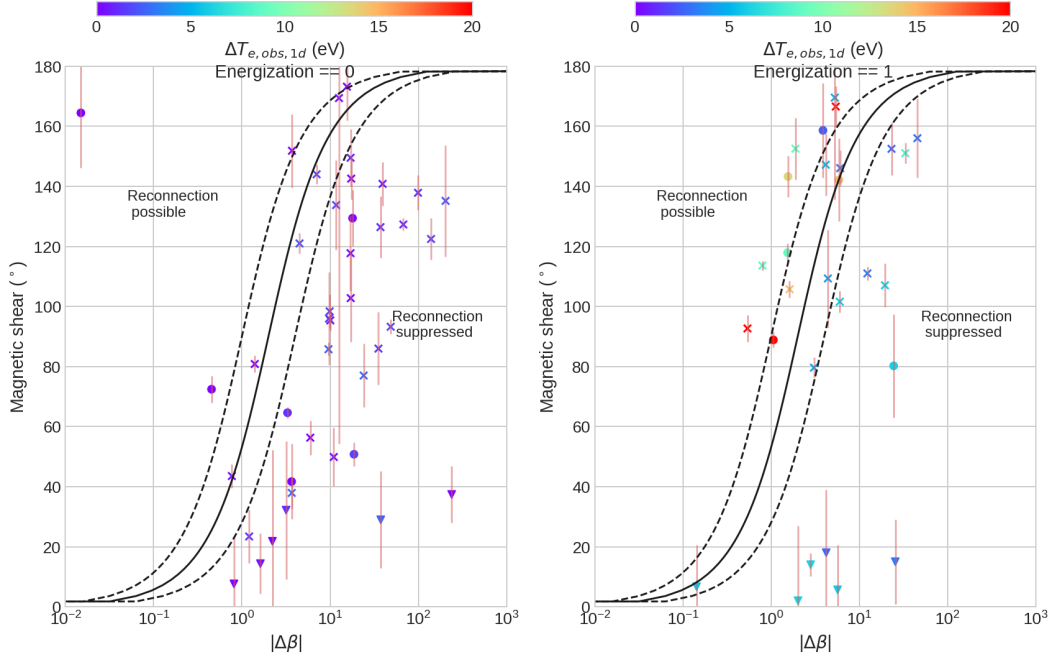


Figure A2: Assessment of diamagnetic suppression of reconnection using the 70 MP crossings with degree of electron heating  $\Delta T_e$  shown as colour scale, including results of error analysis. Format is identical to Figure 8

### 623 Acknowledgments

624 IC was supported by a UK STFC studentship hosted by the UCL centre for Doctoral  
 625 Training in Data Intensive Science. NA and PG were supported by UK STFC Consolidated  
 626 Grant number ST/S000240/1 (UCL/MSSL-Physics and Astronomy Solar System). AM  
 627 was supported by a Royal Society University Research Fellowship. The authors wish to  
 628 thank R.J. Wilson for invaluable discussions and useful comments about this work, and to  
 629 thank G. Lewis for help with CAPS-ELS data. The magnetopause crossings of the Cassini  
 630 spacecraft used in this study were identified and characterised by Masters et al. (2012) using  
 631 the Cassini MAG, ELS, MIMI and IMS data available from the Planetary Data System  
 632 (<http://pds.nasa.gov/>).

### 633 References

- 634 Arridge, C. S., Gilbert, L. K., Lewis, G. R., Sittler, E. C., Jones, G. H., Kataria, D. O., ...  
 635 Young, D. T. (2009). The effect of spacecraft radiation sources on electron moments  
 636 from the Cassini CAPS electron spectrometer. *Planetary and Space Science*, *57*(7),  
 637 854–869. doi: 10.1016/j.pss.2009.02.011  
 638 Baines, K. H., Flasar, F. M., Krupp, N., & Stallard, T. (Eds.). (2018). *Saturn in the 21st*  
 639 *Century*. Cambridge University Press. doi: 10.1017/9781316227220

- 640 Dougherty, M. K., Kellock, S., Southwood, D. J., Balogh, A., Smith, E. J., Tsurutani, B. T.,  
 641 ... Cowley, S. W. (2004, dec). The Cassini magnetic field investigation. *Space Science*  
 642 *Reviews*, *114*(1-4), 331–383. doi: 10.1007/s11214-004-1432-2
- 643 Jackman, C., Thomsen, M., & Dougherty, M. (2019, oct). Survey of Saturn’s magne-  
 644 topause and bow shock positions over the entire Cassini mission: boundary statistical  
 645 properties, and exploration of associated upstream conditions. *Journal of Geophysical*  
 646 *Research: Space Physics*. doi: 10.1029/2019ja026628
- 647 Jasinski, J. M., Arridge, C. S., Lamy, L., Leisner, J. S., Thomsen, M. F., Mitchell, D. G.,  
 648 ... Waite, J. H. (2014). Cusp observation at Saturn’s high-latitude magnetosphere by  
 649 the Cassini spacecraft. *Geophysical Research Letters*, *41*(5), 1382–1388. doi: 10.1002/  
 650 2014GL059319
- 651 Kane, M., Mitchell, D. G., Carbary, J. F., Dialynas, K., Hill, M. E., & Krimigis, S. M. (2020).  
 652 Convection in the Magnetosphere of Saturn During the Cassini Mission Derived From  
 653 MIMI INCA and CHEMS Measurements. *Journal of Geophysical Research: Space*  
 654 *Physics*, *125*(2), 1–21. doi: 10.1029/2019ja027534
- 655 Lewis, G. R., André, N., Arridge, C. S., Coates, A. J., Gilbert, L. K., Linder, D. R.,  
 656 & Rymer, A. M. (2008). Derivation of density and temperature from the Cassini-  
 657 Huygens CAPS electron spectrometer. *Planetary and Space Science*, *56*, 901–912.  
 658 doi: 10.1016/j.pss.2007.12.017
- 659 Masters, A. (2018, aug). A More Viscous-Like Solar Wind Interaction With All the  
 660 Giant Planets. *Geophysical Research Letters*, *45*(15), 7320–7329. doi: 10.1029/  
 661 2018GL078416
- 662 Masters, A., Eastwood, J. P., Swisdak, M., Thomsen, M. F., Russell, C. T., Sergis, N.,  
 663 ... Krimigis, S. M. (2012). The importance of plasma  $\beta$  conditions for magnetic  
 664 reconnection at Saturn’s magnetopause. *Geophysical Research Letters*, *39*(8), 1–6.  
 665 doi: 10.1029/2012GL051372
- 666 McAndrews, H. J., Owen, C. J., Thomsen, M. F., Lavraud, B., Coates, A. J., Dougherty,  
 667 M. K., & Young, D. T. (2008, apr). Evidence for reconnection at Saturn’s mag-  
 668 netopause. *Journal of Geophysical Research: Space Physics*, *113*. doi: 10.1029/  
 669 2007JA012581
- 670 Øieroset, M., Phan, T. D., Fujimoto, M., Lin, R. P., & Lepping, R. P. (2001). In situ  
 671 detection of collisionless reconnection in the Earth’s magnetotail. *Nature*, *412*(6845),  
 672 414–417. doi: 10.1038/35086520
- 673 Phan, T. D., Gosling, J. T., Paschmann, G., Pasma, C., Drake, J. F., Øieroset, M., ...  
 674 Davis, M. S. (2010, aug). The dependence of magnetic reconnection on plasma  $\beta$   
 675 and magnetic shear: Evidence from solar wind observations. *Astrophysical Journal*  
 676 *Letters*, *719*, L199–L203. doi: 10.1088/2041-8205/719/2/L199
- 677 Phan, T. D., Shay, M. A., Gosling, J. T., Fujimoto, M., Drake, J. F., Paschmann, G., ...  
 678 Angelopoulos, V. (2013). Electron bulk heating in magnetic reconnection at Earth  
 679 ’ s magnetopause : Dependence on the in fl ow Alfvén speed and magnetic shear.  
 680 *Geophysical Research Letters*, *40*(17), 4475–4480. doi: 10.1002/grl.50917
- 681 Pierrard, V., & Lazar, M. (2010). Kappa Distributions: Theory and Applications in Space  
 682 Plasmas. *Solar Physics*, *267*(1), 153–174. doi: 10.1007/s11207-010-9640-2

- 683 Pilkington, N. M., Achilleos, N., Arridge, C. S., Guio, P., Masters, A., Ray, L. C., ...  
684 Dougherty, M. K. (2015). Internally driven large-scale changes in the size of Saturn's  
685 magnetosphere. *Journal of Geophysical Research A: Space Physics*, *120*(9), 7289–7306.  
686 doi: 10.1002/2015JA021290
- 687 Pilkington, N. M., Achilleos, N., Arridge, C. S., Masters, A., Sergis, N., Coates, A. J., &  
688 Dougherty, M. K. (2014, apr). Polar confinement of Saturn's magnetosphere revealed  
689 by in situ Cassini observations. *Journal of Geophysical Research: Space Physics*,  
690 *119*(4), 2858–2875. doi: 10.1002/2014JA019774
- 691 Sonnerup, B., Paschmann, G., Papamastorakis, I., Sckopke, N., Haerendel, G., Bame, S. J.,  
692 ... Russell, C. T. (1981). Evidence for magnetic field reconnection at the Earth's  
693 magnetopause. *Journal of Geophysical Research*, *86*(A12), 10049. doi: 10.1029/  
694 ja086ia12p10049
- 695 Sonnerup, B., & Scheible, M. (1998). Minimum and maximum variance analysis. , *001*,  
696 185–220.
- 697 Swisdak, M., Opher, M., Drake, J. F., & Alouani Bibi, F. (2010). The vector direction of  
698 the interstellar magnetic field outside the heliosphere. *Astrophysical Journal*, *710*(2),  
699 1769–1775. doi: 10.1088/0004-637X/710/2/1769
- 700 Swisdak, M., Rogers, B. N., Drake, J. F., & Shay, M. A. (2003, may). Diamagnetic  
701 suppression of component magnetic reconnection at the magnetopause. *Journal of*  
702 *Geophysical Research: Space Physics*, *108*(A5). doi: 10.1029/2002JA009726
- 703 Thomsen, M. F., Reisenfeld, D. B., Delapp, D. M., Tokar, R. L., Young, D. T., Crary,  
704 F. J., ... Williams, J. D. (2010). Survey of ion plasma parameters in Saturn's  
705 magnetosphere. *Journal of Geophysical Research: Space Physics*, *115*(10), 1–22. doi:  
706 10.1029/2010JA015267
- 707 Yamada, M., Kulsrud, R., & Ji, H. (2010). Magnetic reconnection. *Reviews of Modern*  
708 *Physics*, *82*(1), 603–664. doi: 10.1103/RevModPhys.82.603
- 709 Young, D. T., Berthelier, J. J., Blanc, M., Burch, J. L., Bolton, S., Coates, A. J., ... Zins-  
710 meyer, C. (2005). Composition and dynamics of plasma in Saturn's magnetosphere.  
711 *Science*, *307*(5713), 1262–1266. doi: 10.1126/science.1106151
- 712 Young, D. T., Berthelier, J. J., Blanc, M., Burch, J. L., Coates, A. J., Goldstein, R., ...  
713 Zinsmeyer, C. (2004, dec). Cassini plasma spectrometer investigation. *Space Science*  
714 *Reviews*, *114*(1-4), 1–112. doi: 10.1007/s11214-004-1406-4